



ELSEVIER

Available online at www.sciencedirect.com**ScienceDirect**journal homepage: www.elsevier.com/locate/he

Long-term stability of infiltrated $\text{La}_{0.8}\text{Sr}_{0.2}\text{CoO}_{3-\delta}$, $\text{La}_{0.58}\text{Sr}_{0.4}\text{Co}_{0.2}\text{Fe}_{0.8}\text{O}_{3-\delta}$ and $\text{SmBa}_{0.5}\text{Sr}_{0.5}\text{Co}_{2.0}\text{O}_{5+\delta}$ cathodes for low temperature solid oxide fuel cells

Weiting Zhan^{a,b}, Yucun Zhou^b, Ting Chen^b, Guoshuan Miao^b,
Xiaofeng Ye^b, Junliang Li^b, Zhongliang Zhan^b, Shaorong Wang^{b,*},
Zhenyan Deng^a

^a Energy Materials and Physics Group, Department of Physics, Shanghai University, 99 Shangda Road, Shanghai 200444, China

^b CAS Key Laboratory of Materials for Energy Conversion, Shanghai Institute of Ceramics, Chinese Academy of Sciences (SICCAS), 1295 Ding-xi Road, Shanghai 200050, China

ARTICLE INFO

Article history:

Received 5 July 2015

Received in revised form

23 August 2015

Accepted 26 August 2015

Available online 20 October 2015

Keywords:

Solid oxide fuel cells

Infiltration

Stability

Cathodes

ABSTRACT

Here we report the electrochemical performance and long-term stability of $\text{La}_{0.8}\text{Sr}_{0.2}\text{CoO}_{3-\delta}$ (LSC), $\text{La}_{0.58}\text{Sr}_{0.4}\text{Co}_{0.2}\text{Fe}_{0.8}\text{O}_{3-\delta}$ (LSCF) and $\text{SmBa}_{0.5}\text{Sr}_{0.5}\text{Co}_{2.0}\text{O}_{5+\delta}$ (SBSC) infiltrated (ZrO_2)_{0.89}(Sc_2O_3)_{0.1}(CeO_2)_{0.01} (SSZ) cathodes at low temperatures. At 700 °C, the initial polarization resistance of the infiltrated cathodes increased in following order: SBSC-SSZ (0.054 Ω cm²) < LSC-SSZ (0.084 Ω cm²) < LSCF-SSZ (0.140 Ω cm²). After the heat treatment at 620 °C (820–1400 h), the degradation rate of the polarization resistance of LSC-SSZ, LSCF-SSZ and SBSC-SSZ cathode was 179%, 53.9% and 93.1% kh⁻¹, respectively, while that of the ohmic resistance was 10.6%, 8.86% and 40.9% kh⁻¹, respectively. X-ray diffraction (XRD) and scanning electron microscope (SEM) observation showed that the degradation was mainly caused by the morphological change of the infiltrated particles while the solid reactions between the infiltrated materials and SSZ backbones were not observed.

Copyright © 2015, Hydrogen Energy Publications, LLC. Published by Elsevier Ltd. All rights reserved.

Introduction

Solid oxide fuel cells (SOFCs) are energy conversion devices that directly convert chemical energy into electricity with high efficiency and low carbon footprint [1]. Recently, there is a trend to reduce the operation temperature of SOFC to lower temperature (LT) range (<650 °C) in order to reduce system cost, degradation rate as well as start-up and shutdown time

[2]. However, electrochemical impedance of SOFC components will increase with reduced operating temperatures. Infiltration technique is a promising approach for fabricating high performance electrodes with low polarization resistances (R_p) [3–7]. Because the calcination temperature of the infiltrated electrode is much lower than that of the traditional electrode, e.g., 1000–1200 °C for $\text{La}_x\text{Sr}_x\text{Mn}_x\text{O}_x$ (LSM) cathode and 1300–1400 °C for Ni/yttria-stabilized zirconia

* Corresponding author. Tel.: +86 21 66134334; fax: +86 21 66134208.

E-mail address: srwang@mail.sic.ac.cn (S. Wang).

<http://dx.doi.org/10.1016/j.ijhydene.2015.08.073>

0360-3199/Copyright © 2015, Hydrogen Energy Publications, LLC. Published by Elsevier Ltd. All rights reserved.



CrossMark

(YSZ) cermet anode, the grain growth is inhibited, resulting in nano-scale particles deposited into the scaffold. Such nano-scale particles increase the effective length of the triple phase boundaries (TPBs) or the number of the active sites for electrochemical reactions and thus achieve high catalytic activities at low temperatures [2]. In addition, due to the low fabrication temperature of the infiltration technique, the solid reaction between electrode and electrolyte materials can be suppressed in some degree. Also, the infiltrated electrode exhibits an improved matching in coefficient of thermal expansion (CTE) with the electrolyte in comparison with the electrode prepared by screen printing and sintering process [3–7].

The infiltration technique was firstly introduced into the SOFC area by Gorte et al. to prepare the Cu–CeO₂ anode with high tolerance to carbon deposition [8–10]. Subsequently, this technique was widely applied by researchers to make high-performance electrodes. For example, the polarization resistance of the Ni infiltrated La_{0.9}Sr_{0.1}Ga_{0.8}Sm_{0.2}O_{3-d} (LSGM) anode was only 0.011 Ω cm² when measured at 550 °C [11]. Sholklapper et al. have demonstrated the performance improvement by direct loading of LSM nano-particles onto a porous YSZ scaffold [12]. Shao et al. showed that the R_p of Sm_{0.2}Sr_{0.8}CoO_{3-d} infiltrated Sm_{0.2}Ce_{0.8}O_{1.9} (SDC) cathode was only 0.05 Ω cm² at 700 °C [13]. Furthermore, SSC infiltrated LSGM cathode with a low R_p of 0.021 Ω cm² at 650 °C was reported by Han et al. [14].

However, long-term stability of the infiltrated electrode is a critical issue before the successful commercialization of the infiltration technology, even though significant progress has been made in performance enhancement of cell electrodes. Two main reasons will cause the performance degradation of the infiltrated electrodes: firstly, coarsening of infiltrated nano-particles may occur at SOFC operating temperatures, yielding morphological instability [15–19]; secondly, the solid reaction may also occur between the infiltrated material and the scaffold material [13,20]. Tucker et al. reported that the rapid degradation of the cell performance was primarily due to the coarsening of the infiltrated Ni particles [15]. Zhou et al. also showed that coarsening of the nano-scale Ni caused the degradation of the metal-supported fuel cell operating at 650 °C during the 200 h measurement [21]. Han et al. showed that changing infiltrated materials from pure Ni to Ni-SDC mixture produced an improved stability, which was attributed to the restrict growth of Ni by the surrounding SDC [16]. Shao et al. showed that the R_p of Sm_{0.5}Sr_{0.5}CoO_{3-d} (SSC) infiltrated YSZ cathodes increased from 0.09 to 0.55 Ω cm² after a 300 h test at 700 °C, due to the formation of insulating phase of SrZrO₃ and Sm₂Zr₂O₇ [13,20].

Although stability and degradation mechanism of the cathodes like La_{0.6}Sr_{0.4}Co_{0.2}Fe_{0.8}O_{3-d} (LSCF) infiltrated Gd-doped ceria (GDC), LSCF infiltrated YSZ and La_{0.6}Sr_{0.4}CoO_{3-d} (LSC) infiltrated YSZ have been investigated at the temperature range of 700–750 °C, long-term (>1000 h) stability of such cathodes at a lower temperature (~600 °C) have rarely been reported [20,22,23]. In this paper, we studied the electrochemical properties and long-term (800–1400 h) stabilities of La_{0.8}Sr_{0.2}CoO_{3-d} (LSC), La_{0.58}Sr_{0.4}Co_{0.2}Fe_{0.8}O_{3-d} (LSCF) and SmBa_{0.5}Sr_{0.5}Co_{2.0}O_{5+d} (SBSC) infiltrated (ZrO₂)_{0.89}(Sc₂O₃)_{0.1}(CeO₂)_{0.01} (SSZ) cathodes at 550–700 °C.

Experimental

Preparation of cathode materials

The precursor solutions of LSC, LSCF and SBSC were prepared by the Pechini method (citrate method). Stoichiometric amounts of nitrate salts were dissolved into distilled water. Citric acid was then added into the solution with the molar ratio of the citric acid to the total metal ions at 1.5:1. Ammonia was added into the solution to adjust the pH value at ~4 in order to ensure full chelation of citric acid with metal ions. The precursor solutions of LSC, LSCF and SBSC were dried and calcined at 600 °C, 700 °C and 800 °C for 2 h to obtain the corresponding powder. Details for the preparation process can be found in our previous work [16].

Fabrication of symmetrical cells

Commercial SSZ powder ((ZrO₂)_{0.89}(Sc₂O₃)_{0.1}(CeO₂)_{0.01}, Daiichi kigenso kagaku kogyo Co., Ltd Japan) and SDC powder (Sm_{0.2}Ce_{0.8}O_{1.9}, Rarechem high-tech Co., China) with appropriate amounts of dispersant, binder, plasticizer, solvent and other additives were used to obtain the slurries for tape casting. The scaffold of symmetrical cells with a tri-layer structure of “porous SSZ | dense SSZ | porous SSZ” was fabricated by laminating one dense SSZ tape and two porous SSZ tapes on both sides with subsequent co-firing at 1300 °C for 4 h. Thicknesses of the porous SSZ layer and dense SSZ layer were ~40 μm and ~200 μm, respectively. The active area of the symmetrical cells was 0.35 cm². The tri-layer structure of “porous SDC | dense SDC | porous SDC” followed the same process described above. Precursor solutions of LSC, LSCF and SBSC were infiltrated into the porous SSZ scaffold and that of LSCF was infiltrated into the porous SDC scaffold, followed by calcinating at 700 °C for 2 h. The infiltration-calcination process was repeated to achieve desired loadings of the cathode materials. A single infiltration/calcination cycle yielded a loading of ≈5 wt% and the ultimate loading was controlled at 30 wt%.

Electrochemical measurements

Electrochemical impedance spectra (EIS) testing was performed under open-circuit conditions in ambient air using an IM6 Electrochemical Workstation (ZAHNER, Germany) between 100 kHz and 0.1 Hz with a 20 mV perturbation. The ohmic resistance (R₀) was obtained from the value of the high frequency intercept. The electrode polarization resistance (R_p) was measured by the difference between the high and low frequency intersections of the impedance spectra in the first quadrant on the real axis (Zreal axis), and divided by 2 to account for the contributions of two symmetrical electrodes.

Material characterization

The phase structure of synthesized powder was characterized by an X-ray diffraction (XRD, D8 ADVANCE). The diffraction patterns were collected by step scanning in a 2θ range of 20–80° with the scan rate of 10° min⁻¹. To detect potential

phase reaction between infiltrated materials and SSZ at elevated temperatures, the XRD tests of the mixtures of infiltrated materials powder and SSZ powder after firing at 620 °C and 800 °C for 960 h and 100 h, respectively, were conducted. The morphologies of nano-scale cathodes were examined by scanning electron microscope (SEM, Hitachi S-4800-2 and SU-8220).

Results and discussion

XRD patterns of the LSC, LSCF and SBSC powder calcined at 600 °C, 700 °C and 800 °C are shown in Fig. 1(a), (b) and (c),

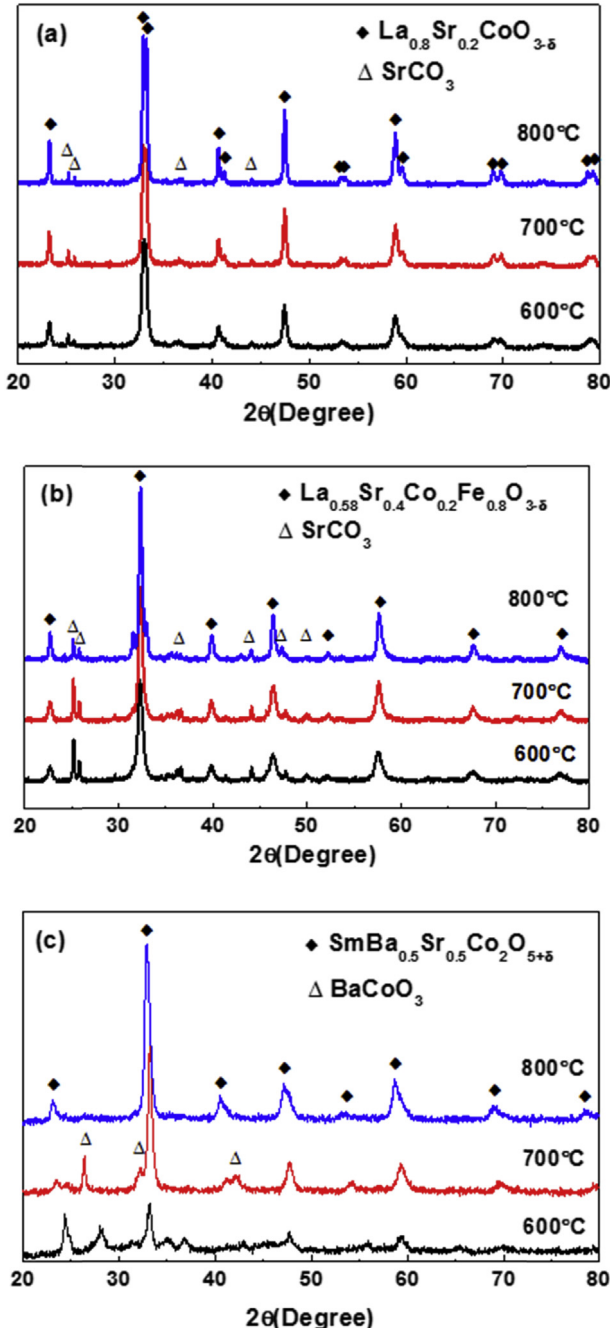


Fig. 1 – XRD patterns of the powder calcined at 600–800 °C: (a) LSC, (b) LSCF, (c) SBSC.

respectively. The dominant phases, perovskite LSC, LSCF and SBSC were formed at the temperature above 700 °C. Small amount of impurities like SrCO₃ in LSC and LSCF, and BaCoO₃ in SBSC could still be found even after increasing the calcinating temperature to 800 °C. In order to avoid the coarsening of the infiltrated nano particles and possible solid reactions between the cathode and the electrolyte materials at a high temperature, the calcinating temperature of infiltrated LSC-SSZ, LSCF-SSZ and SBSC-SSZ cathodes was selected at 700 °C in this study [24–27].

Fig. 2 shows the impedance spectra of the infiltrated cathodes measured in air at 700 °C. As shown in Fig. 2(a), the

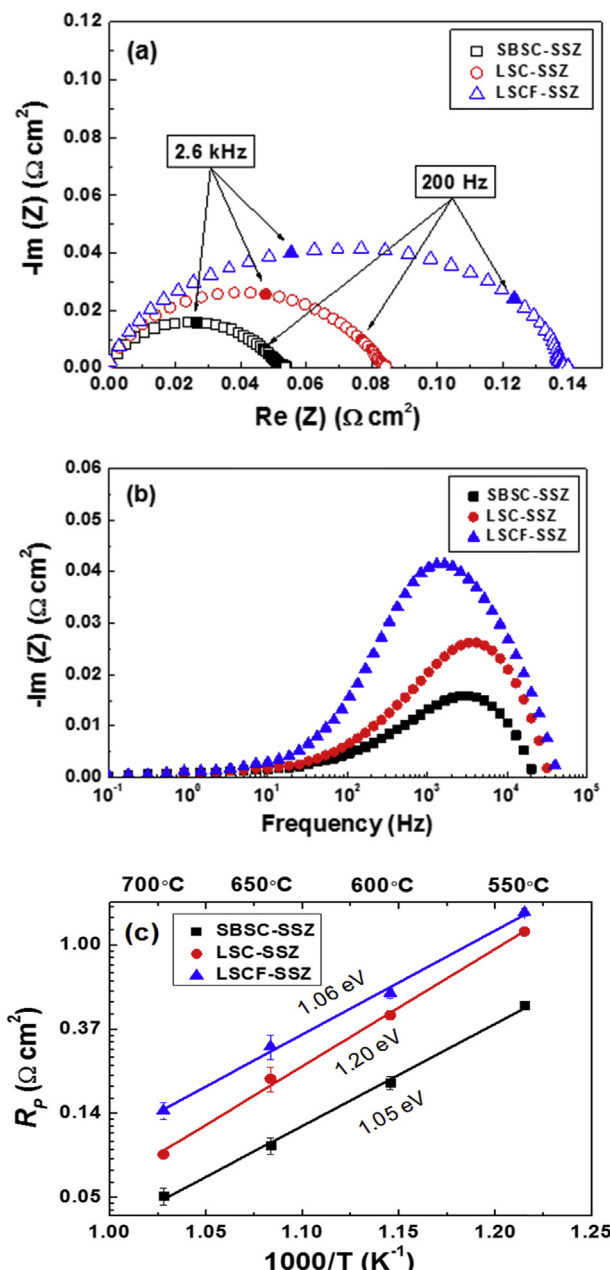


Fig. 2 – Impedance spectra of the infiltrated cathodes measured at 700 °C: (a) Nyquist plots, (b) Bode plots; (c) Polarization resistances of the cathodes as function of temperatures.

R_p values of SBSC-SSZ, LSC-SSZ and LSCF-SSZ were 0.054, 0.084 and 0.140 $\Omega \text{ cm}^2$, respectively. From the Bode plots of the impedance spectra shown in Fig. 2(b), the differences in EIS of different infiltrated cathodes mainly lie in high and medium frequencies. Since the high frequency is usually attributed to the oxygen ion transfer process from the TPB to the electrolyte and the intermediate frequency peak is associated with the surface kinetics [28,29], the differences of the EIS plots can be explained by the different charge transfer and surface processes. As reported, electronic and ionic conductivity of $\text{La}_{0.6}\text{Sr}_{0.4}\text{Co}_{0.2}\text{Fe}_{0.8}\text{O}_{3-\delta}$ at 800 °C was 302 S cm^{-1} and 8×10^{-3} S cm^{-1} , respectively. For $\text{La}_{0.6}\text{Sr}_{0.4}\text{CoO}_{3-\delta}$, the electronic and ionic conductivity (800 °C) could be as high as 1.58×10^3 S cm^{-1} and 0.22 S cm^{-1} , respectively [30]. Since the higher conductivity would facilitate the charge transfer process at the interface of cathode and electrolyte, there is no wonder that the polarization resistance of LSC-SSZ is lower than that of LSCF-SSZ. Fukunaga et al. reported that the oxygen adsorption and desorption processes at the surface of $\text{Sm}_{0.5}\text{Sr}_{0.5}\text{CoO}_3$ was one order of magnitude larger than the corresponding values calculated for $\text{La}_{0.6}\text{Sr}_{0.4}\text{CoO}_3$, which may explain why SBSC-SSZ cathode exhibited the lowest R_p result as shown in Fig. 2(a) [31]. The polarization resistances measured at temperatures from 550 to 700 °C for the infiltrated cathodes are summarized in Fig. 2(c). It shows that the R_p values of the cathodes decreased in following order: LSCF-SSZ > LSC-SSZ > SBSC-SSZ at all measured temperatures. The activation energies of LSC-SSZ, LSCF-SSZ and SBSC-SSZ, calculated from the Arrhenius plots of the fitted line, were 1.20 eV, 1.06 eV and 1.05 eV, respectively.

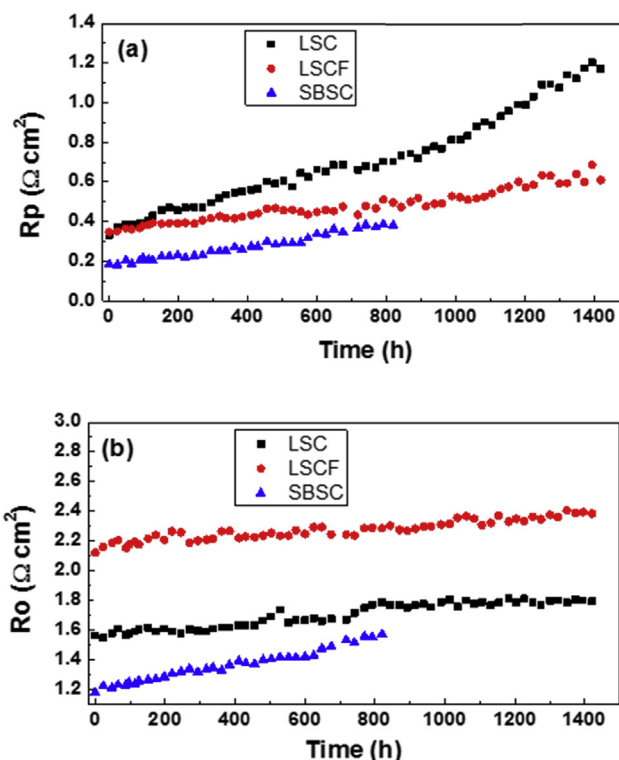


Fig. 3 – Stabilities of the infiltrated cathodes measured at 620 °C: (a) Polarization resistance and (b) Ohmic resistance as a function of the dwelling time.

As shown in Fig. 3, LSC-SSZ and LSCF-SSZ samples were tested at 620 °C for 1400 h and the SBSC-SSZ sample was tested for 820 h. The differences in the initial ohmic losses measured for LSC-SSZ, LSCF-SSZ and SBSC-SSZ were ascribed to the differences in the electrolyte thickness and the electronic conductivity of infiltrated materials. The polarization resistances of LSC-SSZ, LSCF-SSZ and SBSC-SSZ gradually increased from 0.333 to 1.171 $\Omega \text{ cm}^2$, 0.347–0.609 $\Omega \text{ cm}^2$, and 0.186–0.328 $\Omega \text{ cm}^2$, at an average degradation rate of 179% kh^{-1} , 53.9% kh^{-1} , 93.1% kh^{-1} , respectively. While, the ohmic resistances of LSC-SSZ, LSCF-SSZ and SBSC-SSZ increased from 1.561 to 1.792 $\Omega \text{ cm}^2$, 2.121–2.384 $\Omega \text{ cm}^2$ and 1.176–1.570 $\Omega \text{ cm}^2$, at an average degradation rate of 10.6% kh^{-1} , 8.86% kh^{-1} and 40.9% kh^{-1} , respectively. The stability of R_p decreased in the following order: LSCF-SSZ > SBSC-

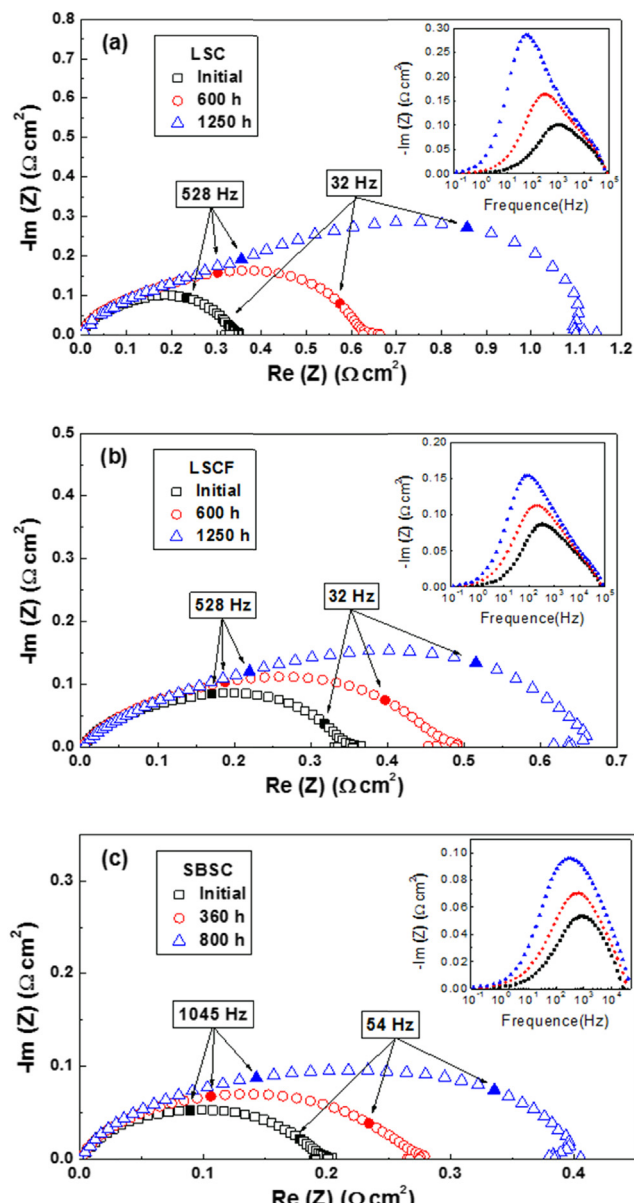


Fig. 4 – Impedance spectra of the infiltrated cathodes measured at 620 °C before and after the stability test: (a) LSC-SSZ, (b) LSCF-SSZ, (c) SBSC-SSZ.

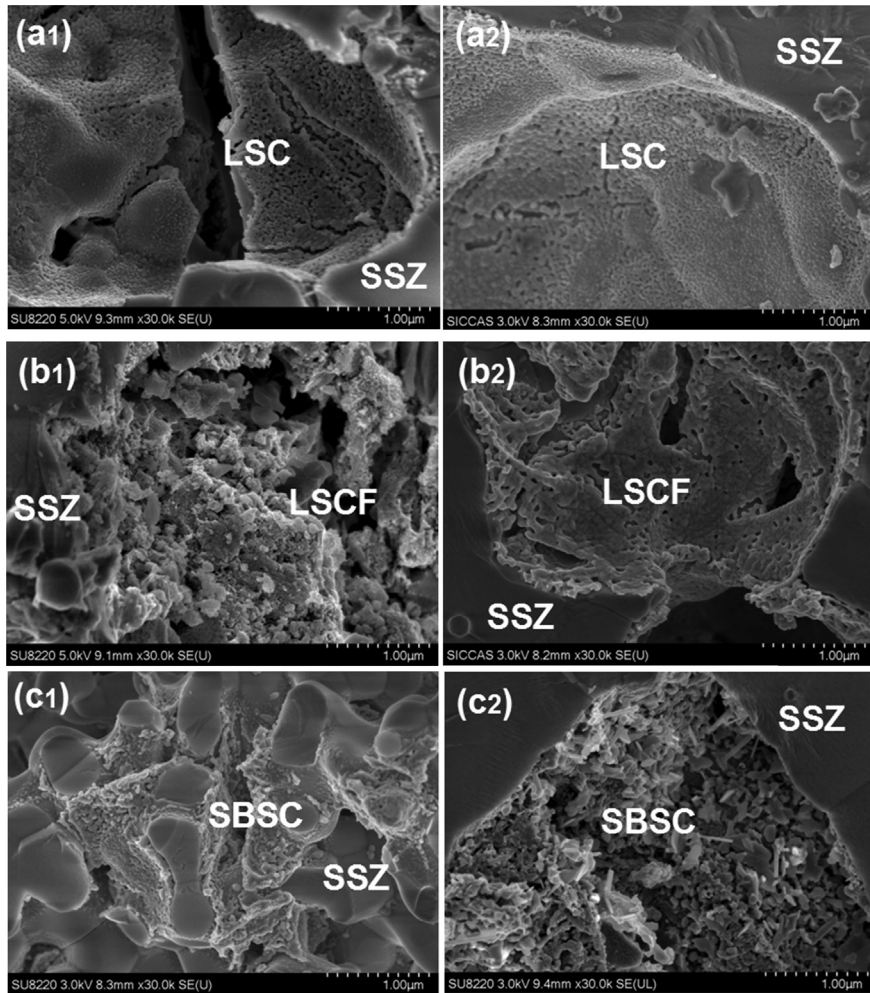


Fig. 5 – SEM images of the cathodes before the stability test: (a1) LSC-SSZ, (b1) LSCF-SSZ, (c1) SBSC-SSZ infiltrated SSZ; SEM images of the cathodes after the stability test: (a2) LSC-SSZ, (b2) LSCF-SSZ, (c2) SBSC-SSZ infiltrated SSZ.

SSZ > LSC-SSZ, with R_o decreasing as LSCF-SSZ > LSC-SSZ > SBSC-SSZ. The increase in R_p was much higher than that in R_o , indicating that polarization resistance dominated the degradation. In order to determine the degradation mechanism, morphology evaluations and solid-state reactions were investigated.

Fig. 4 shows the impedance spectra of the infiltrated cathodes measured with respect to elapsing time. It is seen that the impedance increased gradually and the increase occurred at the medium and low frequencies. Since the intermediate frequency peak is usually associated with the surface kinetics and low frequency is attributed to gas phase diffusion [28,29], the increase of the frequency peak can be explained by the loss of surface-active area for oxygen reduction and the porosity for O_2 gas diffusion.

Fig. 5 shows the SEM micrographs of the LSC-SSZ, LSCF-SSZ and SBSC-SSZ electrodes before and after the stability test. Although the calcination of LSC, LSCF and SBSC infiltrated SSZ scaffold was conducted at the same temperature, the morphology of infiltrated particles were quite different from each other, seen in Fig. 5(a1) (b1) (c1). The micrographs showed that LSC and SBSC particles were evenly distributed

on the surface of the SSZ scaffolds with a particle size of 50–100 nm, whereas LSCF particles agglomerated, sizing from 50 to 500 nm. After the stability test, shown in Fig. 5(a2) (b2) (c2), the LSC and LSCF particles were no longer easily distinguishable, appearing to form a dense polycrystalline layer over the SSZ scaffolds with reduced porosities. The SBSC particles grew dramatically after 820 h, forming rod-like crystallites with the length of 0.1–0.8 μm , agglomerated on the SSZ scaffold. The morphological changes of LSC, LSCF and SBSC decreased the surface areas of the infiltrated phases, which decreased the TPB lengths and porosities, hindered the gas transport process, and thereby increased the R_p values. These results are consistent with the EIS changes shown in Fig. 4. Furthermore, the agglomeration of infiltrated particles led to discrete distribution network on the porous scaffold, disconnecting the current path and thus increasing the R_o values.

To detect the potential reactions between the infiltrated materials and SSZ scaffold, the solid reaction between the cathode powder and SSZ powder was evaluated. The powder of LSC, LSCF and SBSC was synthesized by calcinating at 700 °C for 2 h in air. XRD results shown in Fig. 6(a1), (b1) and

(c1) revealed that no obvious solid reaction occurred for the mixture of LSC + SSZ, LSCF + SSZ and SBSCO + SSZ after the 930 h tests at 620 °C, except for the impurities caused by low calcinating temperature of the starting cathode materials as shown in Fig. 1. Therefore, solid reaction was not the reason for deactivation of the cell performance measured at 620 °C. For comparison, solid reaction became much more obvious by increasing the calcinating temperature to 800 °C. As shown in Fig. 6(a2), (b2) and (c2), after the 100 h heat treatment at 800 °C, secondary phases like SrZrO₃ and La₂Zr₂O₇ formed in the mixture of LSC + SSZ powder, while Co₃O₄, SrZrO₃ in LSCF + SSZ and SmZrO₃, SrZrO₃ and Co₃O₄ in SBSCO + SSZ mixtures. Based upon these XRD results, we can conclude that the increase in R_p and R_o was contributed to the coarsening of the infiltrated particles, not to the formation of insulating phases. Previous studies on the degradation mechanism of the infiltrated cathodes also suggested that coarsening of

infiltrated nano-particles was the main reason to the increased impedance [15–19].

In order to further confirm the conclusion above, LSCF infiltrated SDC cathode was fabricated and measured. Since SDC has good chemically compatibility with the perovskite cathode materials, solid reaction would not be the problem in the LSCF-SDC cathode [32,33]. Fig. 7 shows the impedance values of LSCF infiltrated SDC symmetrical cells measured in air at 650 °C for 820 h. The R_p and R_o results also gradually increased from 0.346 to 1.142 Ω cm², and 4.655–6.084 Ω cm², at an average degradation rate of 280.6% kh⁻¹ and 37.4% kh⁻¹, respectively. Fig. 8 shows the morphology of the infiltrated LSCF particles before and after the stability test. After the 820 h test, well-connected LSCF particles tended to coarsen and form a dense layer. The stability test of LSCF-SDC cell further confirmed that the degradation was mainly caused by the morphological change of the infiltrated particles.

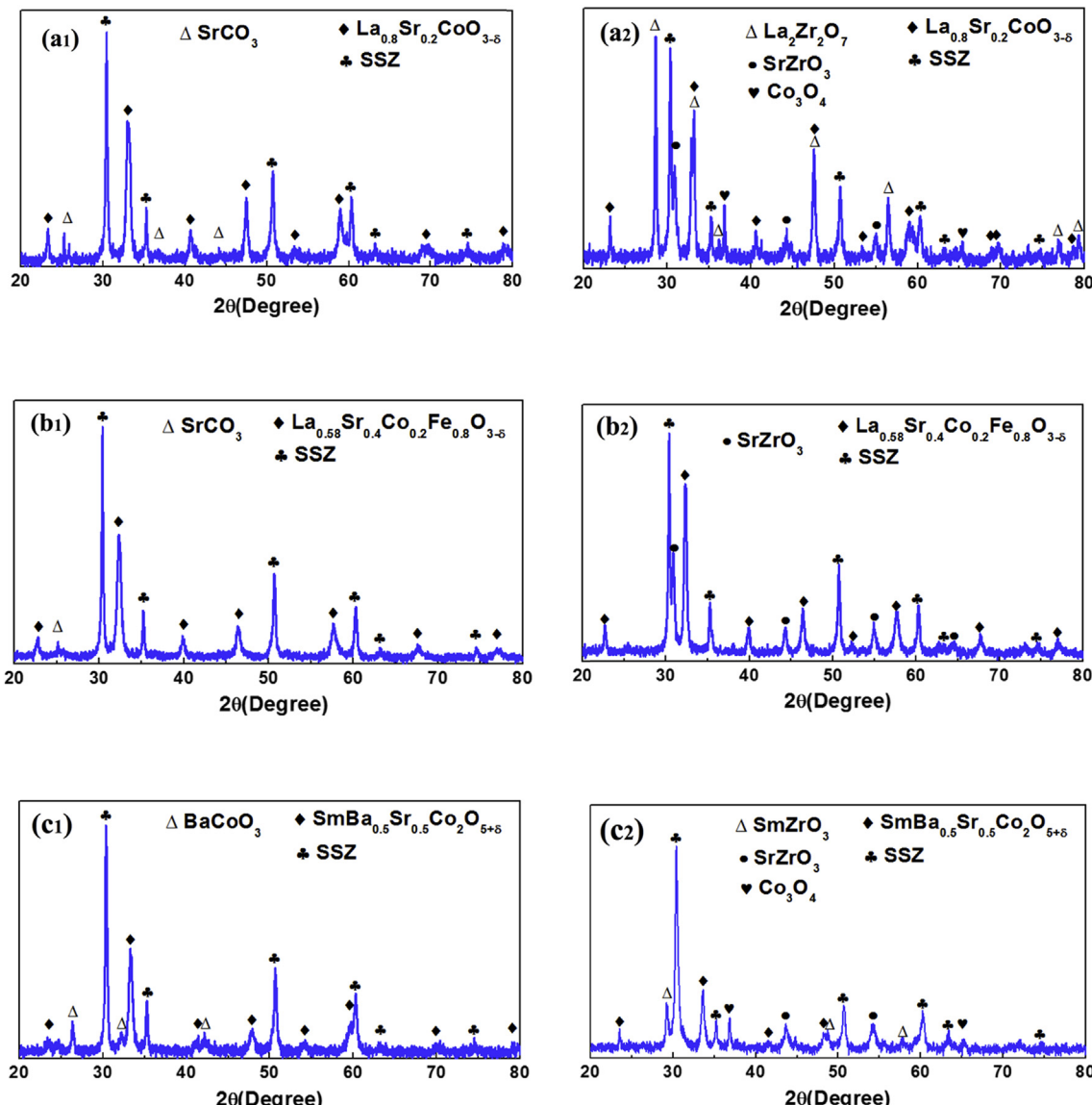


Fig. 6 – XRD patterns of the mixed powder calcined at 620 °C for 930 h: (a1) LSC-SSZ, (b1) LSCF-SSZ, (c1) SBSCO-SSZ; calcined at 800 °C for 100 h: (a2) LSC-SSZ, (b2) LSCF-SSZ, (c2) SBSCO-SSZ.

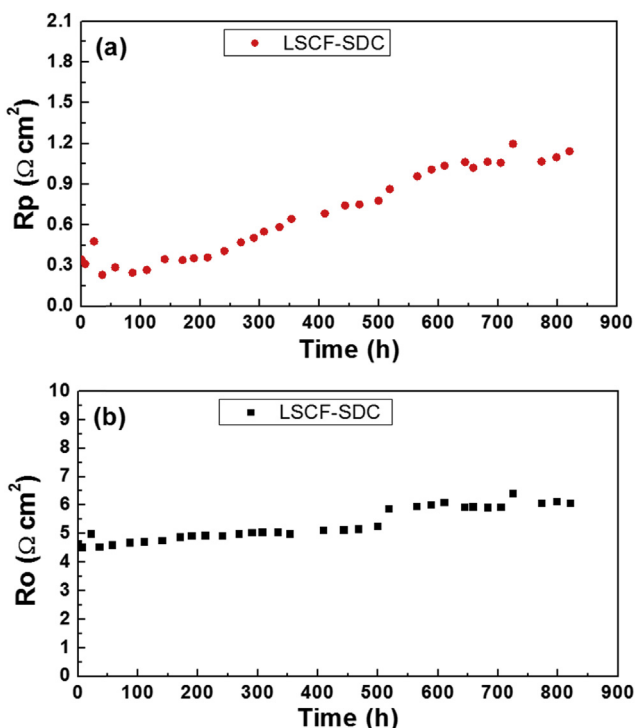


Fig. 7 – Stability of the LSCF-SDC cathode measured at 650 °C: (a) Polarization resistance and (b) Ohmic resistance as a function of the dwelling time.

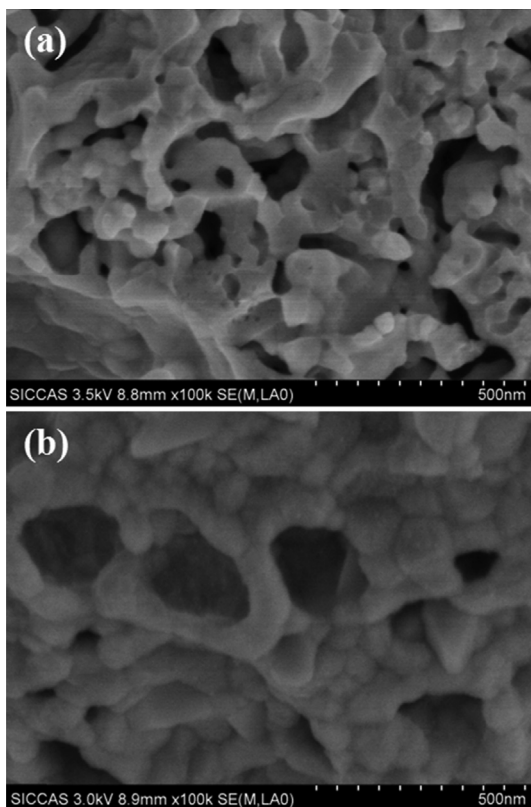


Fig. 8 – SEM images of the infiltrated LSCF particles: (a) Before and (b) after the stability test.

Conclusions

Over the temperature range from 550 to 700 °C, the initial performance of the infiltrated cathodes decreased in the following order: SBSC-SSZ > LSC-SSZ > LSCF-SSZ. Specifically, the R_p value of SBSC-SSZ, LSC-SSZ and LSCF-SSZ at 700 °C was 0.054, 0.084 and 0.140 $\Omega \text{ cm}^2$, respectively. After the 1400 h heat treatment at 620 °C for LSC and LSCF samples, and 820 h for SBSC, the polarization resistances of LSC-SSZ, LSCF-SSZ and SBSC-SSZ gradually increased from 0.333 to 1.171 $\Omega \text{ cm}^2$, 0.347–0.609 $\Omega \text{ cm}^2$, and 0.186–0.328 $\Omega \text{ cm}^2$, at an average degradation rate of 179% kh^{-1} , 53.9% kh^{-1} and 93.1% kh^{-1} , respectively. In the meanwhile, the ohmic resistances for LSC-SSZ, LSCF-SSZ and SBSC-SSZ increased from 1.561 to 1.792 $\Omega \text{ cm}^2$, 2.121–2.384 $\Omega \text{ cm}^2$ and 1.176–1.570 $\Omega \text{ cm}^2$, at an average degradation rate of 10.6% kh^{-1} , 8.86% kh^{-1} and 40.9% kh^{-1} , respectively. After the long-term measurement, the particles tend to form a dense film or the rod-like structure. Considering no obvious solid reactions observed between the infiltrated materials and SSZ after the 930 h test at 620 °C, the main reason for the performance degradation was the morphological change of the infiltrated particles. Notwithstanding the impressive initial performances of these infiltrated cathodes, the performance degradation needs to be further improved, e.g., by co-infiltration [16], to move the technology toward practical applications.

Acknowledgment

We gratefully acknowledge the financial support from the National Natural Science Foundation of China (No.51172266, No.51302301), the Innovation Program of Shanghai Municipal Education Commission (13ZZ079) and the “085 project” of Shanghai Municipal Education Commission.

REFERENCES

- [1] Minh NQ. Ceramic fuel-cells. *J Am Ceram Soc* 1993;76:563–88.
- [2] Wachsman ED, Lee KT. Lowering the temperature of solid oxide fuel cells. *Science* 2011;334:935–9.
- [3] Jiang SP. A review of wet impregnation—An alternative method for the fabrication of high performance and nano-structured electrodes of solid oxide fuel cells. *Mater Sci Eng A* 2006;418:199–210.
- [4] Vohs JM, Gorte RJ. High-performance SOFC cathodes prepared by infiltration. *Adv Mater* 2009;21:943–56.
- [5] Jiang SP. Nanoscale and nano-structured electrodes of solid oxide fuel cells by infiltration: advances and challenges. *Int J Hydrogen Energy* 2012;37:449–70.
- [6] Liu Z, Liu B, Ding D, Liu M, Chen F, Xia C. Fabrication and modification of solid oxide fuel cell anodes via wet impregnation/infiltration technique. *J Power Sources* 2013;237:243–59.
- [7] Ding D, Li X, Lai SY, Gerdes K, Liu M. Enhancing SOFC cathode performance by surface modification through infiltration. *Energy & Environ Sci* 2014;7:552–75.

- [8] Park S, Craciun R, Vohs JM, Gorte RJ. Direct oxidation of hydrocarbons in a solid oxide fuel Cell: I. Methane oxidation. *J Electrochim Soc* 1999;146:3603–5.
- [9] Park SD, Vohs JM, Gorte RJ. Direct oxidation of hydrocarbons in a solid-oxide fuel cell. *Nature* 2000;404:265–7.
- [10] Craciun R, Park S, Gorte RJ, Vohs JM, Wang C, W WL. A novel method for preparing anode cermets for solid oxide fuel cells. *J Electrochim Soc* 1999;146:4019–22.
- [11] Liu X, Meng X, Han D, Wu H, Zeng F, Zhan Z. Impregnated nickel anodes for reduced-temperature solid oxide fuel cells based on thin electrolytes of doped LaGaO₃. *J Power Sources* 2013;222:92–6.
- [12] Sholklapper TZ, Lu C, Jacobson CP, Visco SJ, De Jonghe LC. LSM-infiltrated solid oxide fuel cell cathodes. *Electrochim Solid State Lett* 2006;9. A376–A8.
- [13] Wang F, Chen D, Shao Z. Sm_{0.5}Sr_{0.5}CoO₃-delta-infiltrated cathodes for solid oxide fuel cells with improved oxygen reduction activity and stability. *J Power Sources* 2012;216:208–15.
- [14] Han D, Liu X, Zeng F, Qian J, Wu T, Zhan Z. A micro-nano porous oxide hybrid for efficient oxygen reduction in reduced-temperature solid oxide fuel cells. *Sci Rep* 2012;2.
- [15] Tucker MC, Lau GY, Jacobson CP, DeJonghe LC, Visco SJ. Stability and robustness of metal-supported SOFCs. *J Power Sources* 2008;175:447–51.
- [16] Han D, Liu Y, Wang S, Zhan Z. Enhanced performance of solid oxide fuel cell fabricated by a replica technique combined with infiltrating process. *Int J Hydrogen Energy* 2014;39:13217–23.
- [17] Zhou Y, Xin X, Li J, Ye X, Xia C, Wang S, et al. Performance and degradation of metal-supported solid oxide fuel cells with impregnated electrodes. *Int J Hydrogen Energy* 2014;39:2279–85.
- [18] Liu Y, Chen K, Zhao L, Chi B, Pu J, Jiang SP, et al. Performance stability and degradation mechanism of La_{0.6}Sr_{0.4}Co_{0.2}Fe_{0.8}O_{3-δ} cathodes under solid oxide fuel cells operation conditions. *Int J Hydrogen Energy* 2014;39:15868–76.
- [19] Wang W, Gross MD, Vohs JM, Gorte RJ. The stability of LSF-YSZ electrodes prepared by infiltration. *J Electrochim Soc* 2007;154. B439–B45.
- [20] Huang Y, Ahn K, Vohs JM, Gorte RJ. Characterization of Sr-doped LaCoO₃-YSZ composites prepared by impregnation methods. *J Electrochim Soc* 2004;151. A1592–A7.
- [21] Zhou Y, Yuan C, Chen T, Meng X, Ye X, Li J, et al. Evaluation of Ni and Ni–Ce_{0.8}Sm_{0.2}O_{2-δ} (SDC) impregnated 430L anodes for metal-supported solid oxide fuel cells. *J Power Sources* 2014;267:117–22.
- [22] Liu Y, Wang F, Chi B, Pu J, Jian L, Jiang SP. A stability study of impregnated LSCF–GDC composite cathodes of solid oxide fuel cells. *J Alloys Compd* 2013;578:37–43.
- [23] Liu Y, Chi B, Pu J, Li J. Performance degradation of impregnated La_{0.6}Sr_{0.4}Co_{0.2}Fe_{0.8}O₃+Y₂O₃ stabilized ZrO₂ composite cathodes of intermediate temperature solid oxide fuel cells. *Int J Hydrogen Energy* 2012;37:4388–93.
- [24] Murata K, Fukui T, Abe H, Naito M, Nogi K. Morphology control of La(Sr)Fe(Co)O_{3-a} cathodes for IT-SOFCs. *J Power Sources* 2005;145:257–61.
- [25] Zhou Y, Han D, Yuan C, Liu M, Chen T, Wang S, et al. Infiltrated SmBa_{0.5}Sr_{0.5}Co₂O_{5+δ} cathodes for metal-supported solid oxide fuel cells. *Electrochim Acta* 2014;149:231–6.
- [26] Jørgensen M, Primdahl S, Bagger C, Mogensen M. Effect of sintering temperature on microstructure and performance of LSM–YSZ composite cathodes. *Solid State Ionics* 2001;139:1–11.
- [27] Han D, Wu H, Li J, Wang S, Zhan Z. Nanostructuring of SmBa_{0.5}Sr_{0.5}Co₂O_{5+δ} cathodes for reduced-temperature solid oxide fuel cells. *J Power Sources* 2014;246:409–16.
- [28] Kim J-D, Kim G-D, Moon J-W, Y-i Park, Lee W-H, Kobayashi K, et al. Characterization of LSM–YSZ composite electrode by ac impedance spectroscopy. *Solid State Ionics* 2001;143:379–89.
- [29] Sholklapper TZ, Kurokawa H, Jacobson CP, Visco SJ, De Jonghe LC. Nanostructured solid oxide fuel cell electrodes. *Nano Lett* 2007;7:2136–41.
- [30] Ullmann H, Trofimienko N, Tietz F, Stöver D, Ahmad-Khanlou A. Correlation between thermal expansion and oxide ion transport in mixed conducting perovskite-type oxides for SOFC cathodes. *Solid State Ionics* 2000;138:79–90.
- [31] Fukunaga H, Koyama M, Takahashi N, Wen C, Yamada K. Reaction model of dense Sm_{0.5}Sr_{0.5}CoO₃ as SOFC cathode. *Solid State Ionics* 2000;132:279–85.
- [32] Xu Q, Huang D-p, Zhang F, Chen W, Chen M, Liu H-x. Structure, electrical conducting and thermal expansion properties of La_{0.6}Sr_{0.4}Co_{0.2}Fe_{0.8}O_{3-δ}–Ce_{0.8}Sm_{0.2}O_{2-δ} composite cathodes. *J Alloys Compd* 2008;454:460–5.
- [33] Nie L, Liu M, Zhang Y, Liu M. La_{0.6}Sr_{0.4}Co_{0.2}Fe_{0.8}O_{3-δ} cathodes infiltrated with samarium-doped cerium oxide for solid oxide fuel cells. *J Power Sources* 2010;195:4704–8.